

Graphical Abstract

Beyond PCA: Manifold Dimension Estimation via Local Graph Structure

Bi, Zelong, Lafaye de Micheaux, Pierre

Highlights

Beyond PCA: Manifold Dimension Estimation via Local Graph Structure

Bi, Zelong, Lafaye de Micheaux, Pierre

- We introduce a family of estimators for manifold dimension by integrating PCA with regression techniques, enabling effective capture of intrinsic geometric structure.
- Extensive experiments on both synthetic and real-world datasets demonstrate that our proposed estimators match or outperform state-of-the-art methods across a wide range of settings.

Beyond PCA: Manifold Dimension Estimation via Local Graph Structure

Bi, Zelong^a, Lafaye de Micheaux, Pierre^a

^a*School of Mathematics and Statistics, University of New South Wales, High
St, Kensington, 2052, NSW, Australia*

Abstract

Local principal component analysis (**Local PCA**) has proven to be an effective tool for estimating the intrinsic dimension of a manifold. More recently, curvature-adjusted PCA (**CA-PCA**) has improved upon this approach by explicitly accounting for the curvature of the underlying manifold, rather than assuming local flatness. Building on these insights, we propose a general framework for manifold dimension estimation that characterizes the manifold's local graph structure through the integration of PCA and regression-based techniques. Within this framework, we introduce two representative estimators: quadratic embedding (**QE**) and total least squares (**TLS**). Experiments on both synthetic and real-world datasets demonstrate that these methods perform competitively with, and often outperform, state-of-the-art alternatives.

Keywords: manifold hypothesis, intrinsic dimension estimation, nonlinear dimension reduction, ordinary least squares, total least squares

1. Introduction

Representing high-dimensional data using a significantly smaller number of variables is appealing to both practitioners and theorists. On one hand, many classical methods do not scale well in high-dimensional settings, and working with low-dimensional representations is often more efficient and interpretable. On the other hand, the existence of such representations offers a way to explain the success of modern machine learning techniques, despite the challenges posed by the curse of dimensionality (Keogh and Mueen, 2011).

Traditional dimensionality reduction techniques, such as principal component analysis (PCA, Wold et al. (1987)), typically assume that data points lie in a subspace of the ambient space \mathbb{R}^p . Under this assumption, there exists a global linear map that provides a low-dimensional representation of the entire dataset.

More recent approaches often rely on the more general *manifold hypothesis*, which posits that high-dimensional data lie on or near a low-dimensional manifold embedded in the ambient space (Meilă and Zhang, 2024). In this setting, a global coordinate representation may no longer exist; however, the data can still be locally described using only d ($\leq p$) parameters, where d is the dimension of the underlying manifold. We typically refer to d as the *intrinsic dimension* and p as the *ambient dimension*.

A natural research problem arising from the manifold hypothesis is to estimate this intrinsic dimension d from data—a task commonly referred to as *manifold dimension estimation*. Numerous methods have been proposed across a wide range of domains over the years; see, e.g., Verveer and Duin (1995), Kégl (2002), Yang et al. (2007), Carter et al. (2009), Sricharan et al. (2010), Kalantana and Einbecka (2013), Facco et al. (2017), Lim et al. (2024), and Bi and Lafaye de Micheaux (2025) for a recent survey and numerical comparisons on this topic. Broadly speaking, most manifold dimension estimators are built upon the so-called *flatness assumption*, which approximates local regions of the underlying manifold as d -dimensional linear spaces. This assumption transforms the inherently nonlinear problem into a linear one, enabling the design of numerous estimators.

In Bi and Lafaye de Micheaux (2025), an extensive set of experiments was conducted to benchmark the performance of eight representative methods for manifold dimension estimation. Among them, three emerged as top performers: two are flatness-based—namely, the dimensionality estimator based on angle and norm concentration (**DanCo**, Ceruti et al. (2014)) and the two-nearest-neighbor estimator (**TwoNN**, Facco et al. (2017)); the third is the curvature-adjusted PCA estimator (**CA-PCA**, Gilbert and O’Neill (2025)).

DanCo estimates the intrinsic dimension by analyzing the distributions of pairwise distances and interpoint angles within neighborhoods under the flatness assumption. It further enhances robustness in high-dimensional settings through a Kullback–Leibler (KL) divergence-based comparison framework. **TwoNN** pushes the flatness assumption to its extreme, mitigating curvature effects by relying solely on the two nearest neighbors of each point. Both estimators therefore ignore curvature in local regions. In contrast,

CA-PCA explicitly incorporates curvature information into the local PCA procedure, thus improving upon the already competitive yet often overlooked **Local PCA** estimator (Fukunaga and Olsen, 1971).

Despite their superior performance relative to other estimators, as shown by extensive simulations in Bi and Lafaye de Micheaux (2025), there remains substantial room for improvement: **DanCo** is particularly time-consuming; **TwoNN** tends to underestimate when the intrinsic dimensionality is high, and **CA-PCA** may overestimate the dimension when the manifold is non-linearly embedded in an ambient space of much higher dimension.

Motivated by the strengths and limitations of existing estimators, particularly the robustness of PCA-based approaches and the improvement achieved by **CA-PCA** through its explicit treatment of curvature—we propose a new regression-based framework for manifold dimension estimation. Instead of directly computing geometric quantities from sparse data, our approach recovers the local graph structure of the manifold by regressing normal components on tangent components extracted through PCA from each neighborhood, enabling flexible modeling of curvature and noise.

Our main contributions are as follows:

- **Regression-based formulation.** We introduce a new framework that embeds manifold dimension estimation into a regression setting, allowing complex geometry and noise to be modeled without relying on direct geometric computation. To the best of our knowledge, this perspective is novel in the manifold dimension estimation literature.
- **Representative estimators.** We instantiate the framework with two simple yet effective methods: quadratic embedding (**QE**), a second-order regression model capturing curvature effects, and total least squares (**TLS**), which addresses errors in both predictors and responses.
- **Improved stability and empirical performance.** By reframing dimension estimation as regression, the proposed approach achieves improved robustness and accuracy, particularly in small-sample settings and for manifolds with complex curvature. Extensive experiments on both synthetic and real-world datasets demonstrate that **QE** and **TLS** achieve competitive or superior performance compared to state-of-the-art methods.

The remainder of this article is organized as follows. Section 2 reviews fundamental manifold constructions and introduces our design framework.

Section 3 presents the proposed estimators, followed by experimental results in Section 4. We conclude in Section 5.

2. Manifold Geometry

In this section, we briefly review several fundamental manifold constructions essential for understanding the methods introduced in this article, before presenting our general design framework for manifold dimension estimation. A more comprehensive treatment of the theoretical foundation is provided in Bi and Lafaye de Micheaux (2025). For readers interested in more advanced topics in differential geometry, we refer to Lee (2003, 2018), which offer detailed expositions of the relevant mathematical background.

2.1. Tangent Space and Local Graph Representation

Throughout this article, we take a manifold M as a d -dimensional Riemannian submanifold embedded in an ambient Euclidean space \mathbb{R}^p , generalizing smooth curves and surfaces to higher dimensions. The intrinsic dimension d then refers to the number of free parameters required to describe the manifold locally. That is, for any point $\mathbf{x}_0 \in M$, there exists a neighborhood $U(\mathbf{x}_0) \subseteq M$ that can be smoothly mapped to \mathbb{R}^d via an injective function φ , as illustrated in Figure 1a.

Let φ^{-1} denote the inverse of φ . The *tangent space* of M at \mathbf{x}_0 is defined as the d -dimensional vector space (with operations trivially defined with respect to \mathbf{x}_0) given by

$$T_{\mathbf{x}_0}M = \{\mathbf{x}_0 + d\varphi^{-1}|_{\varphi(\mathbf{x}_0)}(\mathbf{u}) : \mathbf{u} \in \mathbb{R}^d\}.$$

Here, $\mathbf{x}_0 + d\varphi^{-1}|_{\varphi(\mathbf{x}_0)}(\mathbf{u})$ corresponds to the first-order Taylor expansion of φ^{-1} , making $T_{\mathbf{x}_0}M$ the best linear approximation of the manifold near \mathbf{x}_0 , as illustrated in Figure 1b.

The tangent space approximation forms the basis of the widely used *flatness assumption* in manifold dimension estimation. Suppose we are given a data point \mathbf{x}_k along with its K -nearest neighbors sampled from M . The flatness assumption ignores any geometric or distributional irregularities in the neighborhood and posits the data are uniformly distributed within a d -dimensional ball $B_{\mathbf{x}_k}(R) \subseteq T_{\mathbf{x}_k}M$. This local linearization enables the construction of various statistics related to d . In this context, “flatness” refers to ignoring curvature at a local scale.

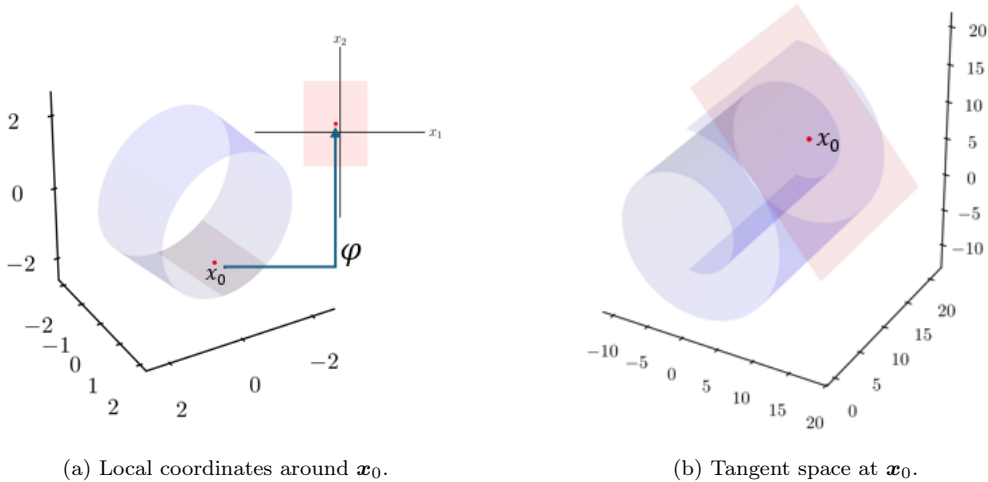


Figure 1: Local coordinate and tangent space.

Furthermore, the neighborhood around \mathbf{x}_0 can be reparameterized to better reflect the manifold’s local geometry. By translating \mathbf{x}_0 to the origin, we can construct a new coordinate system consisting of d orthonormal vectors spanning the tangent space $T_{\mathbf{x}_0}M$, and $p - d$ orthonormal vectors spanning the normal space $(T_{\mathbf{x}_0}M)^\perp$, as shown in Figure 2a. Standard results from differential geometry (Lee, 2003) then guarantee that any point \mathbf{x} sufficiently close to \mathbf{x}_0 can be expressed in these new coordinates as

$$\mathbf{x}' = (\mathbf{x}'_{1:d}, g(\mathbf{x}'_{1:d})), \quad (1)$$

where $\mathbf{x}'_{1:d} = (x'_1, \dots, x'_d)^\top$, $\mathbf{x}'_0 = \mathbf{0}$, and $g: \mathbb{R}^d \rightarrow \mathbb{R}^{p-d}$ is a smooth function satisfying $\nabla g(\mathbf{0}) = \mathbf{0}$.

In this new coordinate system, the neighborhood of \mathbf{x}_0 is represented as the graph of g . The first d components, $\mathbf{x}'_{1:d}$, serve as coordinates in the tangent space, while the remaining $p - d$ components are determined by g and capture deviations from the tangent space approximation. The *flatness assumption* corresponds to the case where $g \doteq 0$, meaning the last $p - d$ coordinates vanish—equivalent to retaining only the first-order Taylor expansion of g around the origin. Consequently, the nontrivial local geometry of the manifold is entirely encoded in the higher-order terms of the Taylor expansion of g . In particular, the second-order Taylor polynomial of g provides a quadratic approximation, as illustrated in Figure 2b.

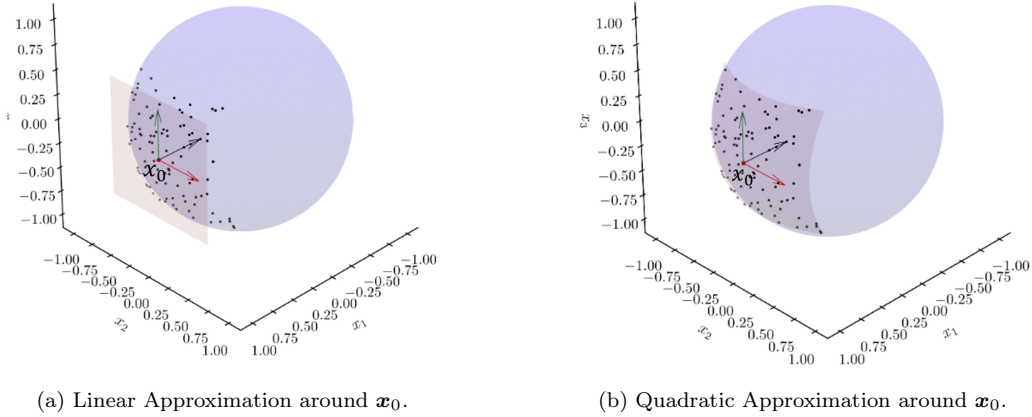


Figure 2: Local Graph Representation.

2.2. Linear and Nonlinear Embedding

A particularly challenging scenario for manifold dimension estimators arises when the underlying manifold M is *space-filling* or *nonlinearly embedded* in the ambient space (Campadelli et al., 2015). Such manifolds typically exhibit more complex curvature. According to the local graph representation discussed above, since there are d linearly independent directions in the tangent space and $p-d$ linearly independent normal directions, a total of $d(p-d)$ values are required to fully describe the curvature at any given point. The more complex the curvature, the more data are needed to accurately capture the underlying geometry, making dimension estimation increasingly difficult.

For example, a 3-dimensional sphere linearly embedded in \mathbb{R}^6 is actually contained within a 4-dimensional subspace, and thus its curvature vanishes in many directions (i.e., g_2 and g_3 are zero, where the g_j are scalar component functions of g). In contrast, consider a 3-dimensional *deformed sphere* embedded in \mathbb{R}^6 , defined via the mapping

$$\varphi^{-1}(\mathbf{u}) = (x_1, \dots, x_6),$$

with

$$x_j = [R + r \cos(2c\pi u_j)] \cos(2\pi u_j), \quad x_{j+3} = [R + r \cos(2c\pi u_j)] \sin(2\pi u_j),$$

for $j = 1, \dots, 3$, where $R, r, c > 0$ are fixed constants. This manifold exhibits nontrivial curvature in all 3×3 tangent and normal directions. Estimati-

ing its intrinsic dimension is therefore significantly more difficult due to the pervasive and nonlinear curvature present in all local neighborhoods.

A major weakness of flatness-based estimators such as **Local PCA** and **DanCo** is their deteriorated performance on nonlinearly embedded manifolds like the deformed sphere. Given the same number of data points in a neighborhood, the flatness assumption is increasingly violated as the curvature becomes more complex.

2.3. Capturing Local Graph Structure

For $j = 1, \dots, p - 1$, let C_j^∞ denote the class of smooth functions with j -dimensional inputs and $(p - j)$ -dimensional outputs. Let \mathcal{M} denote the set of all manifolds embedded in \mathbb{R}^p . A natural way to partition \mathcal{M} is to group its elements according to their intrinsic dimensions. Equivalently, since any j -dimensional manifold can locally be expressed as the graph of a function in C_j^∞ , the set \mathcal{M} can be written as the disjoint union

$$\mathcal{M} = \bigsqcup_{j=1}^p \mathcal{M}_j,$$

where \mathcal{M}_j is the set of all manifolds $M \in \mathcal{M}_j$ that can be locally represented around every point $\mathbf{x}_0 \in M$ as the graph of a map $g_{j,\mathbf{x}_0} \in C_j^\infty$, as in equation (1). Collecting all such local representations gives

$$\mathcal{G}_j := \bigcup_{M \in \mathcal{M}_j} \{g_{j,\mathbf{x}_0} : \mathbf{x}_0 \in M\} \subseteq C_j^\infty,$$

which can be viewed as the space of all smooth local graph representations of j -dimensional manifolds in \mathbb{R}^p .

Given a dataset in \mathbb{R}^p that satisfies the manifold hypothesis, its unknown underlying manifold must belong to one of these subsets \mathcal{M}_j —specifically, to \mathcal{M}_d if its intrinsic dimension is d —and thus be locally represented by \mathcal{G}_d . Our approach to manifold dimension estimation is to identify \mathcal{G}_d .

To operationalize this idea, we specify for each candidate dimension j a family $G_j \subseteq C_j^\infty$ of (parametric) models assumed to be close enough to the functions in \mathcal{G}_j . The data are then fitted to the models in G_j , and a corresponding goodness-of-fit score σ_j is computed to quantify how well each model family explains the data. Ideally, the model is correctly specified (or

best approximated) when $j = d$, resulting in the highest score. Hence, the intrinsic dimension is estimated as

$$\hat{d} = \arg \max_{1 \leq j \leq p} \sigma_j. \quad (2)$$

Details of the model-fitting and evaluation procedures are presented in the next section.

In its most general form, a full model specification may span all p possible partition classes. Within each partition, one may consider multiple families of functions from C_j^∞ , each tailored to model specific local regions of the manifold. The theory guarantees the existence of local graph representation under very mild conditions: it suffices for $g \in C_j^\infty$ to be a smooth function satisfying $\nabla g(\mathbf{0}) = \mathbf{0}$. However, this level of generality is typically too broad to support practical estimation or meaningful model comparison.

To make progress, we must constrain the function classes used to fit data within each partition. The choice of these classes should ideally be guided by our prior knowledge of the underlying manifold. In the absence of such information, a natural default is to take each G_j as a family of quadratic functions. Specifically, we approximate the output of the graph function $g: \mathbb{R}^j \rightarrow \mathbb{R}^{p-j}$ using a tensor of quadratic forms. Let $\mathcal{Q} \in \mathbb{R}^{(p-j) \times j \times j}$ be a third-order tensor, where each slice $\mathcal{Q}[\ell, :, :] = Q_\ell$ is a symmetric matrix encoding the second-order variation of the manifold in the ℓ -th output direction. Then the functions in G_j take the form

$$q_\ell(\mathbf{x}'_{1:j}) = \mathbf{x}'_{1:j}{}^\top Q_\ell \mathbf{x}'_{1:j} = \sum_{i=1}^j \sum_{k=1}^j \mathcal{Q}[\ell, i, k] x'_i x'_k, \quad \ell = 1, \dots, p-j. \quad (3)$$

These quadratic models are not exact in general, but they correspond to the second-order Taylor expansion of the true graph functions, capturing the leading curvature information of the manifold.

We can do better when additional geometric information about the underlying manifold is available. For example, if the manifold is known to be a d -dimensional sphere of radius R (with d , and possibly R , unknown), we can exploit the fact that the local graph function of a sphere has a common structure across different dimensions and local regions:

$$g(\mathbf{x}'_{1:j}) = \left(R - \sqrt{R^2 - \|\mathbf{x}'_{1:j}\|^2}, 0, \dots, 0 \right),$$

where the nonzero component captures the curvature of the sphere. Incorporating such prior knowledge can lead to more accurate modeling than generic quadratic approximations.

To summarize, our proposed framework for manifold dimension estimation enables the construction of a family of estimators based on accurately capturing the local graph structure of the underlying manifold. For each candidate dimension, specific local graph models are specified, guided by prior geometric knowledge. These models are then fitted to the data, and their goodness of fit is evaluated to estimate the intrinsic dimension.

Our framework offers several advantages over existing approaches:

- **Curvature-aware modeling.** By allowing flexible specification of local graph functions—particularly through quadratic forms—we explicitly model the curvature of the underlying manifold. Unlike methods such as **CA-PCA**, which attempt to infer curvature directly from sparse and potentially noisy local samples, our approach embeds the problem into a regression framework, transforming it into a more stable model-fitting task.
- **Model flexibility.** The framework permits highly flexible choices of models for different candidate dimensions, and even allows different models to be used for the same dimension across neighborhoods. This makes it possible to incorporate prior geometric knowledge into model specification. On one end, quadratic models provide a natural default; alternatively, one could consider specifying semiparametric or nonparametric models—such as neural networks—to achieve greater flexibility (Park and Sandberg, 1991). However, such models may be impractical due to the typically limited sample size in each neighborhood, or unnecessarily complex for the specific task of estimating the manifold dimension.
- **Robustness to noise.** The framework naturally accommodates noise modeling, which is critical for real-world datasets. In contrast, many existing manifold dimension estimators are designed under the assumption of clean, noiseless data.

3. Design of New Estimators

The concepts behind **QE** and **TLS** follow naturally from our framework. For both estimators, the model specification for candidate dimensions up to

$p - 1$ is given by the quadratic form in (3). With new coordinates for each neighborhood in hand, the model for dimension j can be fitted by treating the first j coordinates of each data point as inputs and the remaining $p - j$ coordinates as outputs. A local PCA procedure is applied to each neighborhood to estimate the new coordinates guaranteed by the theory, which can be reused across all candidate dimensions. The two estimators differ in their choice of fitting and evaluation methods: **QE** uses ordinary least squares (OLS), while **TLS** employs total least squares (TLS), which accounts for noise in both input and output directions.

3.1. Regression with PCA Coordinates

Following the above discussion, given a data point $\mathbf{x}_k \in \{\mathbf{x}_1, \dots, \mathbf{x}_n\}$ and its K -nearest neighbors $\mathbf{x}_k^1, \dots, \mathbf{x}_k^K$ (ranked by their Euclidean distances from \mathbf{x}_k), we first apply PCA to compute the eigendecomposition of the sample covariance matrix of these $K + 1$ points (after centering them at their local mean, $\bar{\mathbf{x}}_k$). This yields an orthonormal basis whose vectors $\mathbf{v}_1, \dots, \mathbf{v}_p$ are stored in matrix V , with corresponding eigenvalues $\lambda_1 \geq \dots \geq \lambda_p$. Taking the local mean $\bar{\mathbf{x}}_k$ as the new origin, each point in the neighborhood can then be expressed in a new coordinate system aligned with the principal directions, denoted by $\mathbf{x}'_0, \dots, \mathbf{x}'_K$, which are given by

$$\mathbf{x}'_0 = V^\top(\mathbf{x}_k - \bar{\mathbf{x}}_k), \quad \mathbf{x}'_\ell = V^\top(\mathbf{x}_k^\ell - \bar{\mathbf{x}}_k), \quad \ell = 1, \dots, K.$$

By construction, the subspace spanned by $\mathbf{v}_1, \dots, \mathbf{v}_d$ (centered at $\bar{\mathbf{x}}_k$) provides the optimal d -dimensional linear approximation of the data points, in the sense that it minimizes the sum of squared distances from the points to the subspace, among all linear spaces of dimension at most d . This yields a practical linear approximation of the data points, as shown in Figure 3a.



(a) Local linear approximation via PCA.

(b) Local linear approximation via $T_{x_k}M$.

Figure 3: Practical and theoretical local approximations.

On the theoretical side, it is also known that the entire neighborhood around x_k can be approximated by the tangent space at that point, $T_{x_k}M$. Under the local graph representation (1), this corresponds to taking the first-order Taylor approximation of the function g , which is zero. This approximation is illustrated in Figure 3b.

Intuitively, and supported by the strong empirical performance of **Local PCA**—which, at its core, uses the span of principal directions to approximate the tangent space—these two approximations should be close at sufficiently small scales. In other words, the subspace spanned by the first d eigenvectors provides an estimate of the tangent space, up to a small translation and rotation. Indeed, PCA is widely regarded as the most natural method for tangent space estimation; see Lim et al. (2024) for a theoretical discussion of its approximation properties. In subsection 3.3, we also provide a statistical justification of this approximation in the population sense.

For our purposes, the most important consequence is that PCA coordinates provide accurate empirical estimates of the theoretical coordinates involved in the local graph representation (1), thereby allowing us to fit the models corresponding to different candidate dimensions. At its core, our estimator operates by identifying the splitting index d at which a deterministic relationship emerges between the first d coordinates and the remaining $p - d$, governed by the local graph function. The correct intrinsic dimension corresponds to the point where a marked improvement in model fit occurs, thereby revealing the true value of d .

Using the PCA coordinates, recall the quadratic models

$$q_\ell(\mathbf{x}'_{1:j}) = \mathbf{x}'_{1:j}{}^\top Q_\ell \mathbf{x}'_{1:j}, \quad \ell = 1, \dots, p-j, \quad (4)$$

which can be rewritten as linear models by expanding all quadratic and cross-product terms of the inputs $\mathbf{x}'_1, \dots, \mathbf{x}'_j$. For each neighborhood, multivariate linear models such as

$$\mathbf{x}'_{(j+1):p} = (q_1(\mathbf{x}'_{1:j}), \dots, q_{p-j}(\mathbf{x}'_{1:j}))^\top + \boldsymbol{\epsilon}$$

($j = 1, \dots, p-1$) could then be fitted to recover (1) by treating the last $p-j$ PCA coordinates as response variables and applying ordinary least squares (OLS).

Our **QE** estimator simplifies this approach by restricting ourselves to univariate linear models

$$x'_{j+1} = q_1(\mathbf{x}'_{1:j}) + \epsilon.$$

This has two key advantages: first, we avoid PCA coordinates associated with smaller eigenvalues which are typically more sensitive to noise; second, it helps us avoid spurious relationships between input and output when $j < d$. In contrast, using all of the last $p-j$ coordinates as responses introduces the risk of detecting artificial dependencies, which can negatively affect model evaluation.

Our **QE** estimator adopts this approximation but uses only the first output coordinate (i.e., $x'_{k,j+1}$, corresponding to q_1) as the response. This design has several advantages: first, PCA coordinates associated with smaller eigenvalues are typically more sensitive to noise; second, it helps avoid spurious relationships between input and output when $j < d$. In contrast, using all of the last $p-j$ coordinates as responses introduces the risk of detecting artificial dependencies, which can negatively affect model evaluation; lastly, using all output coordinates can easily lead to a combinatorial explosion in the number of parameters, especially when p is large, rendering the models infeasible to fit with the limited data available in neighborhoods.

Our TLS-based estimator (**TLS**) mirrors the structure of **QE**, with the key distinction that the regression step is performed using total least squares (TLS, Golub and Van Loan (1980)) instead of OLS. We also experimented with LASSO (Tibshirani, 1996) and ridge regression (McDonald, 2009) as alternative fitting methods, but found that they yielded inferior performance in this context.

3.2. Filling Details: QE and TLS

Evaluating the model fit is a crucial step within our framework. As (2) suggests, a good fit signals that the intrinsic dimension has likely been reached. For **QE**, this step is straightforward: classical statistical theory provides the F -statistic, specifically designed to compare a target regression model against others.

Figure 4 shows the distribution of F -statistics for $j = 1, 2, 3$, computed from a sample of size 1000 drawn uniformly from a $d = 3$ deformed sphere (with parameter $c = 0.01$). A clear shift of the F -statistic histogram is observed at $j = 3$, demonstrating its potential to accurately identify the intrinsic dimension.

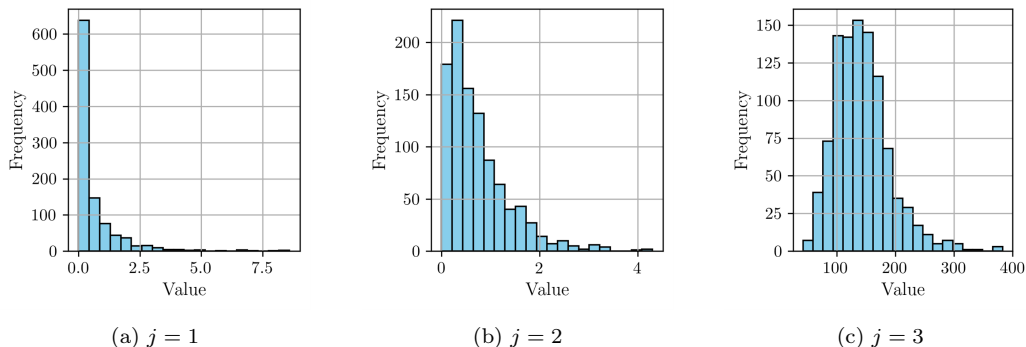


Figure 4: Distribution of F -statistics for different values of j .

In practice, it is often more convenient to base the dimension estimate on the p -value associated with the F -statistic. However, this approach requires care. The validity of the F -distribution hinges on the assumption of normally distributed errors, which may not hold in our setting. Two primary sources of deviation from this assumption exist: (i) error introduced by estimating the tangent space via PCA, and (ii) approximation error in modeling the non-linear map g with a second-order polynomial q . Neither of these guarantees normally distributed residuals, and therefore the theoretical F -distribution may not strictly apply.

Despite this, the F -statistic is well-known for its robustness to different kinds of violations (Box and Watson, 1962; Ali and Sharma, 1996). Empirically, we consistently observe a pronounced jump in its value at the true dimension, and applying a fixed p -value threshold (e.g., at the 1% level) leads to reliable results across a broad range of datasets and settings.

An alternative goodness-of-fit measure that penalizes model complexity is the *adjusted R^2* score. This statistic is bounded above by 1, with larger values indicating better fit. A negative adjusted R^2 suggests that the model performs worse than the trivial model.

The complete **QE** procedure is summarized in Algorithm 1. Beyond the core framework, we incorporate the following refinements:

- Although the first-order Taylor expansion of g_1 is theoretically zero—so its quadratic approximation (the true model) contains only second-order terms—in practice, our PCA coordinates only approximate the theoretical new coordinates in (1). Therefore, we include both first- and second-order terms in the regression to account for the deviation.
- Since $p - 1$ models are fitted in each neighborhood, the procedure can become inefficient when $p \gg d$. In addition to implementation-level optimizations such as parallelization across neighborhoods, we limit the number of models per neighborhood to a maximum of $p_{\max} - 1$. The threshold p_{\max} is determined by three factors: the ambient dimension p ; the largest index for which the standard deviation of the new coordinates is sufficiently large (to avoid fitting near-constant responses); and the neighborhood size K , as regression becomes unreliable when K is smaller than the number of predictors. Letting q denote the largest nonconstant coordinate index, we define¹:

$$p_{\max} = \min \left\{ p, q, \left\lfloor \left(\sqrt{9 + 8K} + 1 \right) / 2 \right\rfloor \right\}. \quad (5)$$

- Each neighborhood yields a local estimate \hat{d}_k , which is the smallest index j such that the p -value of the corresponding F -statistic falls below 1%. To improve robustness, we further require that all models for indices greater than j also yield p -values below the same threshold.
- To compare models across neighborhoods, we record the adjusted R^2 of the model corresponding to each \hat{d}_k . This serves as a joint measure of fit and complexity, and should be close to 1 for a well-fitting model. A local estimate is considered valid only if its adjusted R^2 is positive.

¹When $j = p_{\max} - 1$ components are used as inputs, we need $(p_{\max} - 1)(p_{\max} - 2)/2 + 2(p_{\max} - 1) + 1 \leq K + 1$, which leads to the expression in (5).

The final global estimate \hat{d} is then computed as the weighted average of all valid local estimates \hat{d}_k , with weights proportional to their adjusted R^2 scores.

Algorithm 1 QE

```

1: Input: sample  $\{\mathbf{x}_k\}_{k=1}^n$ ; neighborhood size  $K$ 
2: Output: estimated dimension  $\hat{d}$ 
3: for  $k = 1$  to  $n$  do
4:   Find the  $K$ -nearest neighbors of  $\mathbf{x}_k$ 
5:   Perform PCA on  $\mathbf{x}_k$  and its neighbors; express them in new coordinates as  $\mathbf{x}'_0, \dots, \mathbf{x}'_K$ 
6:   Determine  $p_{\max}$  according to equation (5)
7:   for  $j = 1$  to  $p_{\max}$  do
8:     Fit a quadratic regression model (via OLS) between the first  $j$  coordinates and the  $(j + 1)$ -th
9:     Compute the  $F$ -statistic  $F_j$ , its  $p$ -value  $p_j$ , and the adjusted  $R^2$  score  $w_j$ 
10:    end for
11:    Initialize  $\hat{d}_k = p_{\max}$ ,  $w_k^* = 0$  for  $k = 1, \dots, n$ 
12:    for  $j = 1$  to  $p_{\max}$  do
13:      if  $w_j > 0$  and  $p_i < 1\%$  for all  $i \geq j$  then
14:        Set  $\hat{d}_k = j$ ,  $w_k^* = w_j$ 
15:        break
16:      end if
17:    end for
18:  end for
19: return  $\hat{d} = \sum_k w_k^* \hat{d}_k / \sum_k w_k^*$  (or the unweighted average if all  $w_k^* = 0$ )

```

Compared to ordinary least squares (OLS), the statistical properties of total least squares (TLS) are less well understood. In particular, TLS does not naturally support classical inference tools such as the F -test or adjusted R^2 , making hypothesis testing and model comparison more challenging. In light of this, we can directly evaluate model fit using the total TLS error instead, denoted by σ_{q_j+1} . This quantity corresponds to the sum of squared orthogonal distances from the data points to the best-fit affine subspace. Here, $q_j = j(j - 1)/2 + 2j$ denotes the number of predictors used, account-

ing for both the linear and quadratic terms derived from the first j PCA coordinates.

As in **QE**, the quadratic model is expected to become appropriate only when $j \geq d$. While the total TLS error generally decreases as j increases, a more pronounced drop should be observed at the intrinsic dimension d . However, this drop is not always sharp or immediately discernible. Figure 5 illustrates this behavior for models with $j = 1, \dots, 10$, applied to data sampled from a $d = 10$ sphere. Although the error reaches its minimum at $j = 10$, the decrease from $j = 9$ to $j = 10$ is relatively modest.

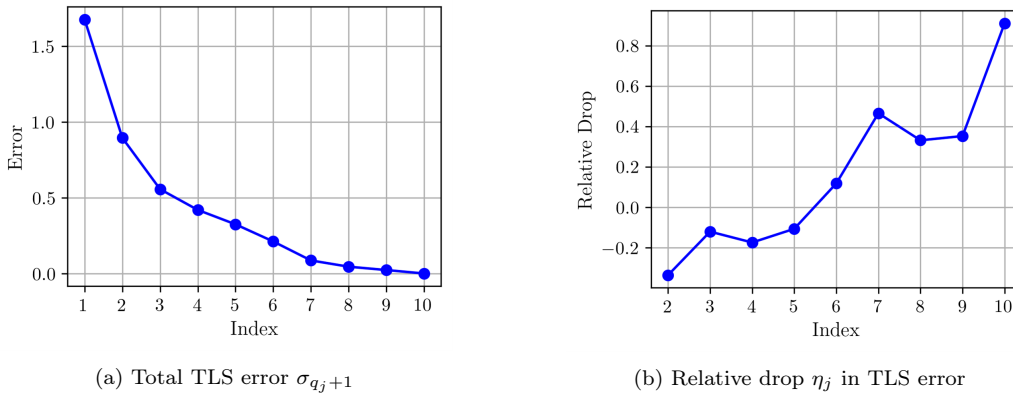


Figure 5: Total TLS error and its relative drops as a function of model dimension.

To improve sensitivity in identifying the intrinsic dimension, we consider the *relative drop* in total error, rather than its absolute value. Specifically, the relative drop from dimension j to $j + 1$ is defined as

$$\eta_{j+1} = \frac{\sigma_{q_j} - \sigma_{q_{j+1}}}{\sigma_{q_j}}, \quad (6)$$

where σ_{q_j} denotes the TLS error associated with dimension j .

As shown in Figure 5b, the relative drop η_j peaks at $j = d$, providing a natural criterion for estimating the local intrinsic dimension \hat{d}_k . Empirically, we find that this approach is robust for $d \geq 2$. However, it is unable to distinguish the case $d = 1$ by design, as there is no $j = 0$ model to compare the total error with.

The complete **TLS** procedure is summarized in Algorithm 2.

Algorithm 2 TLS

- 1: **Input:** sample $\{\mathbf{x}_k\}_{k=1}^n$; neighborhood size K
- 2: **Output:** estimated dimension \hat{d}
- 3: **for** $k = 1$ to n **do**
- 4: Find the K -nearest neighbors of \mathbf{x}_k
- 5: Perform PCA on \mathbf{x}_k and its neighbors; express them in new coordinates as $\mathbf{x}'_0, \dots, \mathbf{x}'_K$
- 6: Determine p_{\max} according to equation (5)
- 7: **for** $j = 1$ to p_{\max} **do**
- 8: Fit a quadratic regression model (via TLS) between the first j coordinates and the $(j + 1)$ -th
- 9: Compute the total error σ_{q_j}
- 10: **end for**
- 11: **for** $j = 2$ to p_{\max} **do**
- 12: Compute the relative drop η_j using equation (6)
- 13: **end for**
- 14: Set $\hat{d}_k = \arg \max_j \{\eta_j\}$
- 15: **end for**
- 16: **return** $\hat{d} = \frac{1}{n} \sum_k \hat{d}_k$

3.3. A Recursive Regression Perspective

Until now, our discussion has proceeded *horizontally*, framing the manifold dimension estimation problem as a model comparison task across different candidate dimensions j . A *vertical* examination of individual dimensions, equipped with specific model specifications, can provide complementary insights.

The local PCA procedure is typically regarded as a direct estimator of the tangent space. However, it also fits naturally within our regression framework. In particular, for $j = d$, if polynomial functions of increasing orders are adopted as models in G_d , then the three estimators—**Local PCA**, **QE**, and **TLS**—can all be interpreted as stages of a unified *recursive regression* scheme, where each stage fits a higher-order term of the local representation function based on the residuals from the previous step. We present this alternative view at the population level, which can be useful as it provides a potential pathway for statistical analysis of these methods.

Let \mathbf{x}_0 be a point on the manifold, and assume its neighborhood $\mathcal{N}_{\mathbf{x}_0}$ can be represented as the graph of a smooth function $g : \mathbb{R}^d \rightarrow \mathbb{R}^{p-d}$. Denote by

$T : \mathbb{R}^p \rightarrow \mathbb{R}^p$ the linear change-of-coordinate mapping such that

$$T(\mathbf{x} - \mathbf{x}_0) = (\mathbf{x}'_{1:d}, g(\mathbf{x}'_{1:d})), \quad \forall \mathbf{x} \in \mathcal{N}_{\mathbf{x}_0}.$$

This coordinate transform provides the starting point of the recursion. It aligns the local coordinates with the manifold geometry so that subsequent regressions can be expressed in these coordinates.

Stage 0: Estimating the coordinate transform. The first step is to estimate T from data in the neighborhood of \mathbf{x}_0 . Since $\mathbf{x}'_{1:d}$ corresponds to the tangent space approximation around \mathbf{x}_0 , at the population level, T should be defined as the solution of

$$\arg \min_{T \in \mathbb{R}^{p \times p}} \mathbb{E}[\|\mathbf{X} - P_d T(\mathbf{X} - \mathbf{x}_0)\|^2 \mid \mathbf{X} \in \mathcal{N}_{\mathbf{x}_0}],$$

where $P_d : \mathbb{R}^p \rightarrow \mathbb{R}^p$ retains the first d components of its input and makes the remaining 0.

When the conditional distribution of \mathbf{X} around \mathbf{x}_0 is approximately uniform or at least isotropic, the solution should coincide with the population PCA, whose columns are the eigenvectors of the local covariance matrix

$$\mathbb{E}_{\mathbf{x}_0}[(\mathbf{X} - \mathbb{E}_{\mathbf{x}_0} \mathbf{X})(\mathbf{X} - \mathbb{E}_{\mathbf{x}_0} \mathbf{X})^\top],$$

where $\mathbb{E}_{\mathbf{x}_0}[\cdot]$ denotes conditional expectation given $\mathbf{X} \in \mathcal{N}_{\mathbf{x}_0}$. This provides a theoretical justification for our use of PCA coordinates to approximate the theoretical new coordinates. Empirically, this corresponds to setting $\mathbf{x}_0 = \mathbf{x}_k$ and replacing population quantities with their sample analogues.

Stage 1: Linear model (no parameters to estimate). After transforming the data via the estimated \hat{T} , we obtain new coordinates $\hat{\mathbf{X}}' = \hat{T}(\mathbf{X} - \mathbf{x}_0)$. At order $m = 1$, the theoretical model is $p_1(\mathbf{x}'_{1:d}) = 0$, which is fully known. Thus, no regression is needed at this stage (i.e., $\hat{p}_1 = 0$)—the linear structure has already been captured by the estimated tangent directions. If we stop here, we end up with **Local PCA**.

Stage 2: Quadratic model. The next step models the nonlinear geometry by fitting a quadratic map in the normal directions. Let

$$p_{2\ell}(\mathbf{x}'_{1:d}) = \mathbf{x}'_{1:d}{}^\top Q_\ell \mathbf{x}'_{1:d}, \quad \ell = 1, \dots, p - d,$$

where $Q_\ell = \nabla^2 g_\ell(\mathbf{0})$. Using $\hat{\mathbf{X}}'$ from the previous step, the goal is to estimate Q_1, \dots, Q_{p-d} by regressing the remaining $p-d$ coordinates on quadratic functions of the first d coordinates. The population-level optimization problem is

$$\arg \min_{Q_\ell \in \mathbb{R}^{d \times d}} \mathbb{E} \left[\sum_{\ell=1}^{p-d} \|\hat{\mathbf{X}}'_{\ell+d} - \hat{\mathbf{X}}'_{1:d}{}^\top Q_\ell \hat{\mathbf{X}}'_{1:d}\|^2 \mid \mathbf{X} \in \mathcal{N}_{\mathbf{x}_0} \right].$$

Importantly, we can view this regression as being performed on the residuals from the previous stage,

$$\hat{\mathbf{X}}'_{(d+1):p} = \hat{\mathbf{X}}'_{(d+1):p} - \hat{p}_1(\hat{\mathbf{X}}'_{1:d}),$$

which formalizes the recursive nature of the procedure.

Our **QE** and **TLS** estimators correspond to the special case of retaining only $\ell = 1$, avoiding the combinatorial growth in the number of parameters. The former employs ordinary least squares, while the latter uses total least squares. Unlike the $m = 1$ stage, the population solution here is not analytically tractable.

Stage 3 and beyond. In principle, one could continue recursively, fitting parameters of a third-order polynomial using the residuals from the quadratic stage,

$$\hat{\mathbf{X}}'_{(d+1):p} - \hat{p}_1(\hat{\mathbf{X}}'_{1:d}) - \hat{p}_2(\hat{\mathbf{X}}'_{1:d}).$$

However, the number of parameters increases rapidly even at $m = 2$. Even accounting for symmetry, the number of coefficients corresponding to the third-order derivatives of g is on the order of $p \times d^3/3!$, making accurate estimation statistically infeasible with local samples. In practice, we almost never go beyond a second-order model.

4. Evaluation

4.1. Setup

In this section, we evaluate the performance of our proposed estimators, **QE** and **TLS**, on a diverse collection of synthetic and real-world datasets. For the synthetic datasets, each experiment is repeated 100 times using randomly generated samples. To assess both bias and variance, we report the mean and standard deviation of the resulting estimates. For comparison, we also

include **Local PCA**, **CA-PCA**, **TwoNN**, and **DanCo**, all of which have been identified as top-performing methods in the existing literature ².

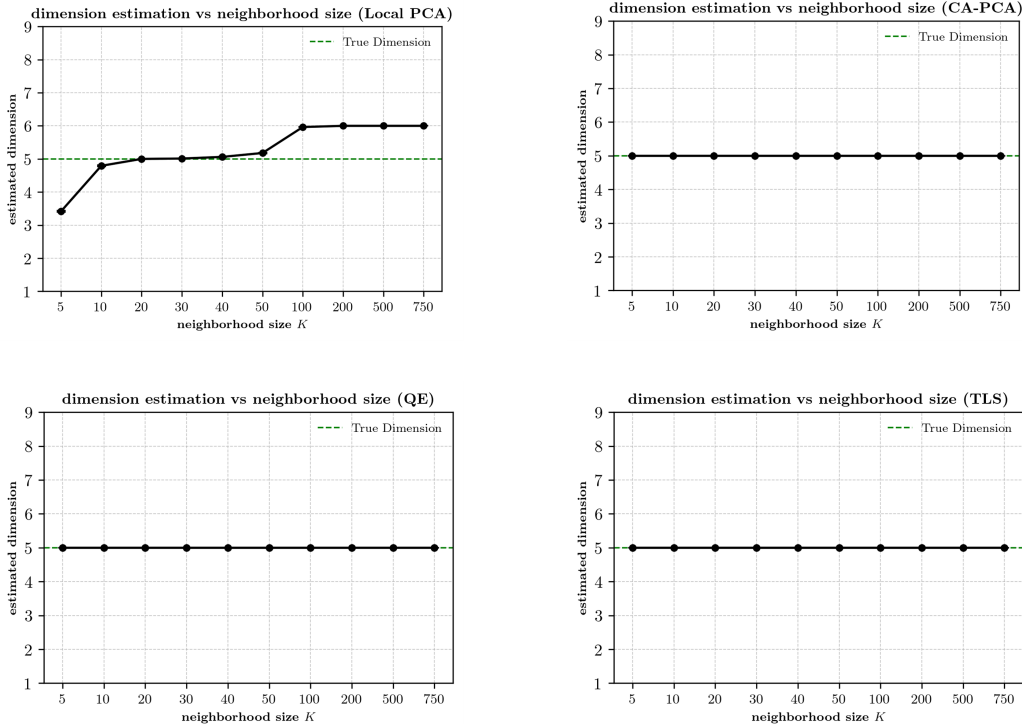


Figure 6: Effect of Neighborhood Size K .

With the exception of **TwoNN**, all evaluated estimators depend on the neighborhood size K as a hyperparameter. The choice of K has a well-documented impact on performance of flatness-based estimators, as it introduces a trade-off: selecting a small K allows for more accurate local linear approximations due to less spread among neighboring points, but may result in insufficient data to reliably capture the underlying geometry. Conversely, a large K can reduce variance but may lead to biased estimates, as the flat-

²Our experiments were conducted using Python. Specifically, we utilized the `skdim` package implementations for **Local PCA**, **TwoNN**, and **DanCo**, while the remaining estimators, as well as the sampling and testing procedures, were implemented by ourselves. The code is available at: <https://github.com/loong-bi/manifold-dimension-estimation>.

ness assumption is violated more. For instance, **DanCo** typically achieves good performance when $K \doteq 10$. The sensitivity of the other estimators to the choice of K is illustrated in Figure 6, based on experiments conducted on datasets of size 1000 uniformly sampled from a 5-dimensional unit sphere linearly embedded in \mathbb{R}^{10} .

Several noteworthy patterns can be observed from Figure 6. As expected for an estimator based on the flatness assumption, the estimates produced by **Local PCA** tend to increase with neighborhood size. This behavior arises because larger neighborhoods capture more of the global geometry, thereby violating the local linear assumption upon which the estimator relies. In contrast, the estimates from **CA-PCA** and our proposed methods, **QE** and **TLS**, remain remarkably stable across the whole range of neighborhood sizes considered. This robustness sets them apart from many existing methods that are sensitive to the choice of K like **Local PCA**.

Since **CA-PCA**, **QE**, and **TLS** all explicitly incorporate curvature into the estimation process, their robustness to neighborhood size suggests that doing so enables more effective modeling of local geometry across a broad range of scales. This property is particularly advantageous for our proposed estimators, which, by design, require sufficiently large neighborhoods to operate reliably. For instance, as noted in Equation 5, when the intrinsic dimension is $d = 10$, a minimum of 15 data points per neighborhood is necessary to avoid premature truncation by p_{\max} . Consequently, it is both essential and beneficial to evaluate our methods over a wide range of neighborhood sizes.

Finally, since the intrinsic dimension is typically unknown in practice, a fair comparison across estimators requires aggregating results over regions of stability in the neighborhood size K . Specifically, we adopt the same approach as in our earlier study: an algorithm searches the hyperparameter space for regions where the standard deviation of the estimates is minimized so that the mean estimates remain approximately constant. If no such stable region is identified, we report the average over all candidate hyperparameter values. For further details, see Bi and Lafaye de Micheaux (2025).

4.2. results

Our first set of experiments evaluates the estimators on 18 synthetic datasets, as described in Table 1. These datasets span a wide range of commonly studied manifolds and are identical to those used in our previous survey. Prior evaluations have shown that **Local PCA**, **CA-PCA**,

DanCo, and **TwoNN** perform well on this benchmark. The results of our experiments are summarized in Tables 2 to 5.

Tables 2 and 3 report results for noiseless, uniformly sampled datasets with sample sizes $n = 500$ and $n = 2000$, respectively. Notably, the selected baseline estimators already perform competitively in this setting. Nonetheless, our proposed estimators demonstrate comparable or superior performance in many cases—particularly when the sample size is small, where competing methods tend to exhibit greater bias and variance, especially on nonlinearly embedded manifolds (M_{41} to M_{43}).

However, our methods encounter difficulties on trivial manifolds such as hyperballs (M_{21} to M_{23}). This is expected, as both **QE** and **TLS** are designed to fit local quadratic models, which are ill-suited for trivial manifolds with zero curvature, i.e., the quadratic model (4) misspecifies. In these cases, the estimators revert to their fallback mechanisms, which are less effective.

Tables 4 and 5 present results for the same set of synthetic datasets with added p -dimensional Gaussian noise. As expected, the presence of noise leads to a substantial degradation in performance across nearly all estimators. Nevertheless, in many cases, our proposed estimators continue to outperform existing methods, benefiting from the robustness of the underlying regression procedures, which explicitly account for noise. In comparison, most existing estimators base their design on the noiseless setup.

In particular, the performance of our **TLS** estimator improves significantly with larger sample sizes, indicating that explicitly modeling noise in both the predictors and responses can be beneficial in noisy settings. It is also noteworthy that even the top-performing methods exhibit considerable bias on relatively simple manifolds such as M_6 to M_{10} , underscoring the inherent difficulty of the dimension estimation task in the presence of noise.

One of the main motivations for explicitly incorporating curvature into the design of manifold dimension estimators is the potential for improved performance on nonlinearly embedded manifolds—i.e., manifolds exhibiting nontrivial curvature in all directions. Such cases are particularly challenging for estimators that rely on local flatness assumptions. The deformed spheres (M_{41} to M_{43}) serve as representative examples of this category.

To further evaluate this aspect, we conducted experiments on six additional manifolds generated using the `skdim` library. These manifolds are all nonlinearly embedded in higher-dimensional ambient spaces and are specifically chosen for their increased geometric complexity. Details of these datasets

are provided in Table 6, with the corresponding results presented in Tables 7 and 8 for sample sizes $n = 500$ and $n = 2000$, respectively.

Among these datasets, the top-performing estimators turn out to be **TwoNN**, **QE**, and **TLS**. In contrast, **Local PCA** and **DanCo** exhibit weaker performance, which is expected given their reliance on the flatness assumption and lack of explicit curvature modeling. Interestingly, despite accounting for curvature, **CA-PCA** also performs poorly—particularly on manifolds where the ambient dimension significantly exceeds the intrinsic dimension, often leading to overestimation. This observation is consistent with findings from our previous survey. A possible reason might be its relying—at least partially—on detecting a gap between significant and negligible eigenvalues. When many small but nonzero eigenvalues are present due to curvature or noise, the distinction becomes blurred, often misleading the estimator and degrading performance.

Lastly, we evaluate our estimators on three real-world datasets commonly used in manifold dimension estimation studies. The first is the **ISOMAP** dataset, which consists of 698 grayscale images (64×64 pixels) of a face sculpture and is believed to have an intrinsic dimension of approximately 3. The second is a subset of the **MNIST** dataset, comprising 6,742 grayscale images of the digit "1" (each of size 28×28), with an estimated intrinsic dimension between 8 and 11. The third is the **ISOLET** dataset, which contains 6,240 vectors of length 616, representing frequency-based features extracted from audio recordings of spoken English letters, and is believed to have an intrinsic dimension between 16 and 22. The corresponding results are presented in Tables 9, 10, and 11³.

In all three datasets, the ambient dimension substantially exceeds the intrinsic dimension, resulting in significant overestimation by both **Local PCA** and **CA-PCA**. While **TwoNN** provides estimates close to the expected values for the **ISOMAP** and **MNIST** datasets, it tends to underestimate the intrinsic dimension for **ISOLET**, as anticipated given the higher underlying dimensionality. In contrast, the estimates produced by **DanCo** and **QE** fall within the expected ranges for all three datasets. Our **TLS** estimator

³The results reported for **DanCo**, shown in brackets, are taken from Ceruti et al. (2014) and Campadelli et al. (2015), which include implementation-specific adjustments designed to stabilize performance. A direct application of **DanCo** using the `skdim` library does not reproduce these results; see Bi and Lafaye de Micheaux (2025) for further discussion.

also yields results that are consistently close to these expected values, further demonstrating its robustness across a range of real-world scenarios.

5. Conclusion

This article introduces a design paradigm for manifold dimension estimators that aims to effectively recover the local graph structure of the manifold by performing regression on PCA coordinates. Two representative estimators—**QE** and **TLS**—are described in detail. Both approximate the local graph structure through a quadratic model; **QE** employs ordinary least squares, while **TLS** uses total least squares, providing robustness to noise in both predictors and responses. Extensive experiments on synthetic and real-world datasets demonstrate that both methods perform on par with, and often outperform, leading state-of-the-art estimators. Their advantages are especially pronounced in settings with limited sample sizes or nonlinear embeddings in high-dimensional ambient spaces.

With a better understanding of the underlying manifold, one could make more informed choices of the functions G_j , potentially leading to estimators that achieve improved performance for specific tasks beyond the two proposed in this work. However, the absence of suitable diagnostic tools currently prevents us from doing so. It remains unclear which sample statistics would provide meaningful guidance in selecting appropriate forms of G_j . Further research on this question—both theoretical and practical—is needed to advance this direction.

Acknowledgements

This research includes computations using the computational cluster Katana supported by Research Technology Services at UNSW Sydney.

This paper is part of Z. Bi’s Ph.D. thesis.

6. Appendix: Tables of Results

Table 1: The 18 manifolds used in Tables 2–5.

Manifold	Description
M_{11}	A 5-dimensional sphere embedded in \mathbb{R}^{10} with $R = 1$.
M_{12}	A 10-dimensional sphere embedded in \mathbb{R}^{20} with $R = 1$.
M_{13}	A 20-dimensional sphere embedded in \mathbb{R}^{40} with $R = 1$.
M_{21}	A 5-dimensional ball embedded in \mathbb{R}^{10} with $R = 1$.
M_{22}	A 10-dimensional ball embedded in \mathbb{R}^{20} with $R = 1$.
M_{23}	A 20-dimensional ball embedded in \mathbb{R}^{40} with $R = 1$.
M_{31}	A 5-dimensional Gaussian density surface embedded in \mathbb{R}^{10} corresponding to $N(0, 0.25I_5)$.
M_{32}	A 10-dimensional Gaussian density surface embedded in \mathbb{R}^{20} corresponding to $N(0, 0.25I_{10})$.
M_{33}	A 20-dimensional Gaussian density surface embedded in \mathbb{R}^{40} corresponding to $N(0, 0.25I_{20})$.
M_{41}	A 3-dimensional deformed sphere with $c = 0.01$.
M_{42}	A 3-dimensional deformed sphere with $c = 0.1$.
M_{43}	A 3-dimensional deformed sphere with $c = 1$.
M_5	A 2-dimensional cylinder embedded in \mathbb{R}^4 .
M_6	A 1-dimensional helix embedded in \mathbb{R}^3 .
M_7	A 2-dimensional Swiss roll embedded in \mathbb{R}^4 .
M_8	A 2-dimensional Mobius strip embedded in \mathbb{R}^4 .
M_9	A 2-dimensional torus embedded in \mathbb{R}^4 .
M_{10}	A 2-dimensional hyperbolic surface embedded in \mathbb{R}^4 .

Table 2: Mean dimension estimates (\pm standard deviation) for 18 manifolds (Table 1) with true dimension d , based on 100 replicates of $n = 500$ uniform samples. Bold indicates the estimate with minimal MSE.

Manifold	Local PCA	CA-PCA	DanCo	TwoNN	QE	TLS
$M_{11}(5)$	5.00 \pm 0.00	5.03 \pm 0.01	6.18 \pm 0.26	4.90 \pm 0.28	5.00 \pm 0.00	5.00 \pm 0.00
$M_{12}(10)$	10.21 \pm 0.02	10.10 \pm 0.01	11.16 \pm 0.37	9.17 \pm 0.53	10.00 \pm 0.00	10.00 \pm 0.00
$M_{13}(20)$	20.68 \pm 0.02	19.76 \pm 0.02	20.13 \pm 0.37	15.90 \pm 0.90	20.00 \pm 0.00	19.99 \pm 0.00
$M_{21}(5)$	4.91 \pm 0.03	5.00 \pm 0.00	4.97 \pm 0.13	4.64 \pm 0.30	4.72 \pm 0.28	2.86 \pm 0.04
$M_{22}(10)$	9.93 \pm 0.03	9.99 \pm 0.01	10.03 \pm 0.17	8.79 \pm 0.51	9.84 \pm 0.29	5.19 \pm 0.18
$M_{23}(20)$	19.93 \pm 0.02	19.10 \pm 0.04	20.01 \pm 0.28	15.53 \pm 0.92	19.49 \pm 0.44	18.17 \pm 0.17
$M_{31}(5)$	5.00 \pm 0.01	5.00 \pm 0.00	4.97 \pm 0.13	4.55 \pm 0.27	5.00 \pm 0.00	5.00 \pm 0.00
$M_{32}(10)$	10.01 \pm 0.02	10.00 \pm 0.00	9.55 \pm 0.39	8.28 \pm 0.51	10.05 \pm 0.16	10.00 \pm 0.00
$M_{33}(20)$	20.07 \pm 0.05	19.43 \pm 0.04	19.59 \pm 0.54	14.75 \pm 0.83	20.85 \pm 0.22	20.00 \pm 0.00
$M_{41}(3)$	3.24 \pm 0.02	5.83 \pm 0.02	3.42 \pm 0.12	3.05 \pm 0.17	3.00 \pm 0.00	3.17 \pm 0.03
$M_{42}(3)$	3.25 \pm 0.02	5.83 \pm 0.02	3.44 \pm 0.12	3.05 \pm 0.17	3.00 \pm 0.00	3.13 \pm 0.02
$M_{43}(3)$	3.44 \pm 0.03	5.52 \pm 0.05	3.58 \pm 0.14	3.06 \pm 0.16	3.00 \pm 0.00	3.47 \pm 0.04
$M_5(2)$	1.95 \pm 0.01	2.00 \pm 0.00	2.16 \pm 0.03	1.98 \pm 0.12	2.00 \pm 0.00	2.00 \pm 0.00
$M_6(1)$	1.00 \pm 0.00	2.75 \pm 0.04	1.01 \pm 0.02	1.00 \pm 0.07	1.97 \pm 0.01	2.00 \pm 0.00
$M_7(2)$	2.78 \pm 0.04	2.99 \pm 0.01	2.18 \pm 0.03	1.97 \pm 0.12	2.00 \pm 0.00	2.00 \pm 0.00
$M_8(2)$	1.93 \pm 0.01	2.00 \pm 0.00	2.18 \pm 0.03	1.96 \pm 0.12	2.00 \pm 0.00	2.00 \pm 0.00
$M_9(2)$	2.00 \pm 0.01	3.00 \pm 0.00	2.16 \pm 0.03	2.00 \pm 0.13	2.00 \pm 0.00	2.00 \pm 0.00
$M_{10}(2)$	1.95 \pm 0.01	2.07 \pm 0.01	2.18 \pm 0.03	1.99 \pm 0.12	2.00 \pm 0.00	2.00 \pm 0.00

Table 3: Mean dimension estimates (\pm standard deviation) for 18 manifolds (Table 1) with true dimension d , based on 100 replicates of $n = 2000$ uniform samples. Bold indicates the estimate with minimal MSE.

Manifold	Local PCA	CA-PCA	DanCo	TwoNN	QE	TLS
$M_{11}(5)$	5.00 \pm 0.00	5.00 \pm 0.00	6.54 \pm 0.17	4.97 \pm 0.14	5.00 \pm 0.00	5.00 \pm 0.00
$M_{12}(10)$	10.00 \pm 0.00	10.01 \pm 0.00	10.92 \pm 0.14	9.40 \pm 0.24	10.00 \pm 0.00	10.00 \pm 0.00
$M_{13}(20)$	20.17 \pm 0.01	19.70 \pm 0.01	19.97 \pm 0.24	16.74 \pm 0.52	20.00 \pm 0.00	19.94 \pm 0.01
$M_{21}(5)$	4.93 \pm 0.01	5.00 \pm 0.00	5.00 \pm 0.06	4.76 \pm 0.14	4.31 \pm 0.27	2.68 \pm 0.02
$M_{22}(10)$	9.91 \pm 0.02	9.99 \pm 0.00	10.00 \pm 0.11	8.96 \pm 0.22	9.92 \pm 0.21	4.13 \pm 0.06
$M_{23}(20)$	19.79 \pm 0.03	19.00 \pm 0.03	19.98 \pm 0.15	16.17 \pm 0.43	19.45 \pm 0.39	18.18 \pm 0.05
$M_{31}(5)$	5.00 \pm 0.00	5.00 \pm 0.00	5.11 \pm 0.08	4.68 \pm 0.13	5.00 \pm 0.00	5.00 \pm 0.00
$M_{32}(10)$	10.00 \pm 0.00	10.00 \pm 0.00	9.71 \pm 0.31	8.61 \pm 0.25	10.00 \pm 0.00	10.00 \pm 0.00
$M_{33}(20)$	19.99 \pm 0.01	19.38 \pm 0.02	20.87 \pm 0.37	15.41 \pm 0.38	20.10 \pm 0.19	20.00 \pm 0.00
$M_{41}(3)$	3.00 \pm 0.00	3.11 \pm 0.01	2.99 \pm 0.05	3.03 \pm 0.09	3.00 \pm 0.00	3.00 \pm 0.00
$M_{42}(3)$	3.00 \pm 0.00	3.12 \pm 0.01	3.01 \pm 0.05	3.03 \pm 0.09	3.00 \pm 0.00	3.00 \pm 0.00
$M_{43}(3)$	3.01 \pm 0.00	3.17 \pm 0.01	3.76 \pm 0.09	3.03 \pm 0.09	3.00 \pm 0.00	3.02 \pm 0.01
$M_5(2)$	1.97 \pm 0.00	2.00 \pm 0.00	2.14 \pm 0.02	1.97 \pm 0.05	2.00 \pm 0.00	2.00 \pm 0.00
$M_6(1)$	1.00 \pm 0.00	1.00 \pm 0.00	1.00 \pm 0.00	1.00 \pm 0.03	1.00 \pm 0.00	2.00 \pm 0.00
$M_7(2)$	1.98 \pm 0.01	2.03 \pm 0.00	2.16 \pm 0.01	1.97 \pm 0.06	2.00 \pm 0.00	2.00 \pm 0.00
$M_8(2)$	1.96 \pm 0.00	2.00 \pm 0.00	2.15 \pm 0.01	1.97 \pm 0.05	2.00 \pm 0.00	2.00 \pm 0.00
$M_9(2)$	2.00 \pm 0.00	2.00 \pm 0.00	2.15 \pm 0.02	2.00 \pm 0.06	2.00 \pm 0.00	2.00 \pm 0.00
$M_{10}(2)$	1.98 \pm 0.00	2.00 \pm 0.00	2.16 \pm 0.01	1.98 \pm 0.06	2.00 \pm 0.00	2.00 \pm 0.00

Table 4: Mean dimension estimates (\pm standard deviation) for 18 manifolds (Table 1) with true dimension d , based on 100 replicates of $n = 500$ uniform samples perturbed by Gaussian noise. Bold indicates the estimate with minimal MSE.

Manifold	Local PCA	CA-PCA	DanCo	TwoNN	QE	TLS
$M_{11}(5)$	7.35 ± 0.32	7.19 ± 0.07	7.49 ± 0.24	6.99 ± 0.35	8.40 ± 0.21	5.55 ± 0.01
$M_{12}(10)$	19.06 ± 0.06	13.27 ± 0.08	14.69 ± 0.41	11.98 ± 0.61	11.06 ± 0.15	11.61 ± 0.01
$M_{13}(20)$	35.93 ± 0.07	25.73 ± 0.11	34.36 ± 1.01	20.84 ± 1.13	21.05 ± 0.13	19.99 ± 0.00
$M_{21}(5)$	9.89 ± 0.03	8.77 ± 0.08	8.22 ± 0.22	7.52 ± 0.43	5.77 ± 0.19	8.15 ± 0.01
$M_{22}(10)$	19.50 ± 0.04	15.20 ± 0.12	14.65 ± 0.57	12.25 ± 0.63	10.71 ± 0.12	11.79 ± 0.02
$M_{23}(20)$	36.23 ± 0.08	25.89 ± 0.12	35.01 ± 1.25	21.03 ± 0.97	20.38 ± 0.12	19.99 ± 0.00
$M_{31}(5)$	5.06 ± 0.03	5.04 ± 0.02	6.02 ± 0.15	5.66 ± 0.33	5.74 ± 0.15	6.06 ± 0.01
$M_{32}(10)$	10.22 ± 0.08	10.00 ± 0.00	10.16 ± 0.28	8.93 ± 0.50	11.04 ± 0.11	10.64 ± 0.00
$M_{33}(20)$	21.15 ± 0.24	19.55 ± 0.03	20.42 ± 0.57	15.28 ± 0.76	20.10 ± 0.19	19.99 ± 0.00
$M_{41}(3)$	3.44 ± 0.03	5.90 ± 0.01	4.04 ± 0.14	3.47 ± 0.18	3.00 ± 0.00	3.06 ± 0.01
$M_{42}(3)$	3.46 ± 0.03	5.90 ± 0.01	4.07 ± 0.14	3.48 ± 0.18	3.01 ± 0.01	3.03 ± 0.01
$M_{43}(3)$	3.89 ± 0.05	5.79 ± 0.03	4.73 ± 0.19	3.88 ± 0.19	3.71 ± 0.10	3.58 ± 0.06
$M_5(2)$	3.52 ± 0.10	3.93 ± 0.01	4.00 ± 0.00	3.85 ± 0.21	3.50 ± 0.36	2.79 ± 0.02
$M_6(1)$	1.73 ± 0.04	2.97 ± 0.01	2.94 ± 0.09	2.77 ± 0.15	1.96 ± 0.01	2.00 ± 0.00
$M_7(2)$	2.78 ± 0.04	2.99 ± 0.01	2.27 ± 0.04	2.18 ± 0.11	2.49 ± 0.45	2.45 ± 0.02
$M_8(2)$	3.20 ± 0.10	3.94 ± 0.02	4.00 ± 0.02	3.75 ± 0.20	3.04 ± 0.38	2.81 ± 0.02
$M_9(2)$	2.10 ± 0.01	3.00 ± 0.00	2.89 ± 0.13	2.98 ± 0.15	2.94 ± 0.67	2.74 ± 0.02
$M_{10}(2)$	2.15 ± 0.04	3.19 ± 0.06	3.86 ± 0.16	3.29 ± 0.18	3.14 ± 0.39	2.95 ± 0.01

Table 5: Mean dimension estimates (\pm standard deviation) for 18 manifolds (Table 1) with true dimension d , based on 100 replicates of $n = 2000$ uniform samples perturbed by Gaussian noise. Bold indicates the estimate with minimal MSE.

Manifold	Local PCA	CA-PCA	DanCo	TwoNN	QE	TLS
$M_{11}(5)$	9.78 ± 0.04	8.40 ± 0.03	10.00 ± 0.02	7.77 ± 0.20	7.33 ± 0.01	5.52 ± 0.01
$M_{12}(10)$	19.60 ± 0.02	14.56 ± 0.05	14.89 ± 0.21	13.03 ± 0.32	13.00 ± 0.01	10.60 ± 0.01
$M_{13}(20)$	35.38 ± 0.04	26.17 ± 0.05	36.49 ± 0.90	22.68 ± 0.64	21.00 ± 0.00	21.00 ± 0.00
$M_{21}(5)$	9.99 ± 0.00	9.61 ± 0.02	10.00 ± 0.00	8.25 ± 0.24	5.67 ± 0.03	8.09 ± 0.03
$M_{22}(10)$	19.83 ± 0.01	16.21 ± 0.06	15.02 ± 0.13	13.33 ± 0.30	11.66 ± 0.01	12.75 ± 0.01
$M_{23}(20)$	35.68 ± 0.04	26.38 ± 0.06	37.51 ± 0.96	22.81 ± 0.58	20.00 ± 0.00	19.99 ± 0.00
$M_{31}(5)$	5.08 ± 0.02	5.87 ± 0.05	6.97 ± 0.09	6.34 ± 0.17	6.33 ± 0.01	6.16 ± 0.01
$M_{32}(10)$	10.09 ± 0.02	10.00 ± 0.00	10.49 ± 0.33	9.47 ± 0.27	11.66 ± 0.01	10.63 ± 0.00
$M_{33}(20)$	20.27 ± 0.04	19.52 ± 0.02	22.82 ± 0.62	16.13 ± 0.37	20.33 ± 0.00	19.99 ± 0.00
$M_{41}(3)$	3.03 ± 0.00	3.85 ± 0.02	4.46 ± 0.12	3.93 ± 0.10	3.00 ± 0.00	3.00 ± 0.00
$M_{42}(3)$	3.04 ± 0.01	3.89 ± 0.02	4.52 ± 0.13	3.96 ± 0.10	3.00 ± 0.00	3.00 ± 0.00
$M_{43}(3)$	3.53 ± 0.04	4.55 ± 0.03	5.04 ± 0.19	4.47 ± 0.14	3.17 ± 0.03	3.68 ± 0.03
$M_5(2)$	3.98 ± 0.00	4.00 ± 0.00	4.00 ± 0.00	4.00 ± 0.12	3.07 ± 0.16	2.77 ± 0.01
$M_6(1)$	2.54 ± 0.01	2.85 ± 0.01	3.00 ± 0.00	3.01 ± 0.08	2.05 ± 0.14	2.00 ± 0.00
$M_7(2)$	1.99 ± 0.01	2.13 ± 0.01	2.39 ± 0.02	2.50 ± 0.07	2.52 ± 0.15	2.67 ± 0.01
$M_8(2)$	3.96 ± 0.01	4.00 ± 0.00	4.00 ± 0.00	3.97 ± 0.11	3.14 ± 0.23	2.77 ± 0.01
$M_9(2)$	2.17 ± 0.02	3.52 ± 0.02	3.98 ± 0.07	3.54 ± 0.10	2.66 ± 0.16	2.95 ± 0.01
$M_{10}(2)$	3.07 ± 0.04	3.87 ± 0.01	4.00 ± 0.00	3.76 ± 0.10	3.04 ± 0.14	2.87 ± 0.01

Table 6: The 6 nonlinearly embedded manifolds used in Tables 7–8.

Manifold	Description
M_{NL1}	A 6-dimensional paraboloid nonlinearly embedded in \mathbb{R}^{21} .
M_{NL2}	A 4-dimensional manifold (concentrated figure) nonlinearly embedded in \mathbb{R}^6 .
M_{NL3}	A 4-dimensional manifold nonlinearly embedded in \mathbb{R}^6 .
M_{NL4}	A 10-dimensional manifold nonlinearly embedded in \mathbb{R}^{40} .
M_{NL5}	A 12-dimensional manifold nonlinearly embedded in \mathbb{R}^{72} .
M_{NL6}	An 18-dimensional manifold nonlinearly embedded in \mathbb{R}^{72} .

Table 7: Mean dimension estimates (\pm standard deviation) for 6 nonlinearly embedded manifolds (Table 6) with true dimension d , based on 100 replicates of $n = 500$ samples. Bold indicates the estimate with minimal MSE.

Manifold	Local PCA	CA-PCA	DanCo	TwoNN	QE	TLS
$M_{\text{NL}1}(6)$	7.26 ± 0.21	5.68 ± 0.05	5.48 ± 0.16	3.61 ± 0.06	5.99 ± 0.01	6.36 ± 0.03
$M_{\text{NL}2}(4)$	4.64 ± 0.09	5.16 ± 0.07	4.90 ± 0.20	3.67 ± 0.05	4.66 ± 0.05	4.56 ± 0.05
$M_{\text{NL}3}(4)$	7.65 ± 0.05	7.44 ± 0.06	6.00 ± 0.28	4.75 ± 0.04	5.26 ± 0.10	6.93 ± 0.01
$M_{\text{NL}4}(10)$	24.17 ± 0.84	9.08 ± 0.11	6.36 ± 0.19	4.78 ± 0.10	9.08 ± 0.15	10.96 ± 0.02
$M_{\text{NL}5}(12)$	25.25 ± 0.36	21.06 ± 0.08	18.71 ± 0.79	11.52 ± 0.12	11.98 ± 0.02	12.92 ± 0.01
$M_{\text{NL}6}(18)$	25.52 ± 0.25	18.04 ± 0.03	18.28 ± 0.74	11.25 ± 0.09	18.00 ± 0.00	18.00 ± 0.00

Table 8: Mean dimension estimates (\pm standard deviation) for 6 nonlinearly embedded manifolds (Table 6) with true dimension d , based on 100 replicates of $n = 2000$ samples. Bold indicates the estimate with minimal MSE.

Manifold	Local PCA	CA-PCA	DanCo	TwoNN	QE	TLS
$M_{\text{NL}1}(6)$	6.34 ± 0.06	5.91 ± 0.02	6.61 ± 0.15	4.63 ± 0.03	5.99 ± 0.00	6.36 ± 0.02
$M_{\text{NL}2}(4)$	4.44 ± 0.04	4.98 ± 0.03	5.09 ± 0.20	3.92 ± 0.03	4.59 ± 0.02	4.72 ± 0.02
$M_{\text{NL}3}(4)$	4.42 ± 0.02	6.28 ± 0.03	5.53 ± 0.18	4.42 ± 0.02	4.16 ± 0.02	6.87 ± 0.01
$M_{\text{NL}4}(10)$	16.07 ± 0.32	9.16 ± 0.04	7.00 ± 0.05	5.42 ± 0.04	9.34 ± 0.05	10.92 ± 0.01
$M_{\text{NL}5}(12)$	23.92 ± 0.04	20.33 ± 0.05	17.36 ± 0.31	12.77 ± 0.06	10.98 ± 0.01	12.92 ± 0.00
$M_{\text{NL}6}(18)$	22.31 ± 0.06	17.89 ± 0.01	20.73 ± 0.53	12.73 ± 0.05	17.00 ± 0.01	18.00 ± 0.00

Table 9: Dimension Estimate on Real-world Datasets: ISOMAP

Local PCA	CA-PCA	DanCo	TwoNN	QE	TLS
10.05	25.71	(4.00)	3.49	3.07	3.44

Table 10: Dimension Estimate on Real-world Datasets: MNIST

Local PCA	CA-PCA	DanCo	TwoNN	QE	TLS
15.41	84.66	(9.98)	12.98	9.23	6.73

References

Ali, M.M., Sharma, S.C., 1996. Robustness to nonnormality of regression f-tests. *Journal of Econometrics* 71, 175–205.

Table 11: Dimension Estimate on Real-world Datasets: ISOLET

Local PCA	CA-PCA	DanCo	TwoNN	QE	TLS
34.44	54.22	(19.00)	9.11	17.51	25.42

- Bi, Z., Lafaye de Micheaux, P.L., 2025. Manifold dimension estimation: An empirical study. arXiv preprint arXiv:2509.15517 .
- Box, G.E., Watson, G.S., 1962. Robustness to non-normality of regression tests. *Biometrika* 49, 93–106.
- Campadelli, P., Casiraghi, E., Ceruti, C., Rozza, A., 2015. Intrinsic dimension estimation: Relevant techniques and a benchmark framework. *Mathematical Problems in Engineering* 2015, 759567.
- Carter, K.M., Raich, R., Hero III, A.O., 2009. On local intrinsic dimension estimation and its applications. *IEEE Transactions on Signal Processing* 58, 650–663.
- Ceruti, C., Bassis, S., Rozza, A., Lombardi, G., Casiraghi, E., Campadelli, P., 2014. Danco: An intrinsic dimensionality estimator exploiting angle and norm concentration. *Pattern Recognition* 47, 2569–2581.
- Facco, E., d’Errico, M., Rodriguez, A., Laio, A., 2017. Estimating the intrinsic dimension of datasets by a minimal neighborhood information. *Scientific reports* 7, 12140.
- Fukunaga, K., Olsen, D.R., 1971. An algorithm for finding intrinsic dimensionality of data. *IEEE Transactions on computers* 100, 176–183.
- Gilbert, A.C., O’Neill, K., 2025. Ca-pca: Manifold dimension estimation, adapted for curvature. *SIAM Journal on Mathematics of Data Science* 7, 355–383.
- Golub, G.H., Van Loan, C.F., 1980. An analysis of the total least squares problem. *SIAM journal on numerical analysis* 17, 883–893.
- Kalantana, J.E.Z., Einbecka, Z., 2013. Intrinsic dimensionality estimation for high-dimensional data sets: New approaches for the computation of correlation dimension. *J. Emerg. Technol. Web Intell* 5, 91–97.

- Kégl, B., 2002. Intrinsic dimension estimation using packing numbers. *Advances in neural information processing systems* 15.
- Keogh, E., Mueen, A., 2011. Curse of dimensionality, in: *Encyclopedia of machine learning*. Springer, pp. 257–258.
- Lee, J.M., 2003. Smooth manifolds, in: *Introduction to smooth manifolds*. Springer, pp. 1–29.
- Lee, J.M., 2018. *Introduction to Riemannian manifolds. volume 2*. Springer.
- Lim, U., Oberhauser, H., Nanda, V., 2024. Tangent space and dimension estimation with the wasserstein distance. *SIAM Journal on Applied Algebra and Geometry* 8, 650–685.
- McDonald, G.C., 2009. Ridge regression. *Wiley Interdisciplinary Reviews: Computational Statistics* 1, 93–100.
- Meilă, M., Zhang, H., 2024. Manifold learning: What, how, and why. *Annual Review of Statistics and Its Application* 11, 393–417.
- Park, J., Sandberg, I.W., 1991. Universal approximation using radial-basis-function networks. *Neural computation* 3, 246–257.
- Sricharan, K., Raich, R., Hero, A.O., 2010. Optimized intrinsic dimension estimator using nearest neighbor graphs, in: *2010 IEEE International Conference on Acoustics, Speech and Signal Processing, IEEE*. pp. 5418–5421.
- Tibshirani, R., 1996. Regression shrinkage and selection via the lasso. *Journal of the Royal Statistical Society Series B: Statistical Methodology* 58, 267–288.
- Verveer, P.J., Duin, R.P.W., 1995. An evaluation of intrinsic dimensionality estimators. *IEEE Transactions on pattern analysis and machine intelligence* 17, 81–86.
- Wold, S., Esbensen, K., Geladi, P., 1987. Principal component analysis. *Chemometrics and intelligent laboratory systems* 2, 37–52.
- Yang, X., Michea, S., Zha, H., 2007. Conical dimension as an intrinsic dimension estimator and its applications, in: *Proceedings of the 2007 SIAM International Conference on Data Mining, SIAM*. pp. 169–179.